ISSN 0915-633X

NATIONAL INSTITUTE FOR FUSION SCIENCE

Interaction of Cover and Target with Xenon Gas in the IFE-Reaction Chamber

Boris V. Kuteev

(Received - Oct. 10, 2001)

NIFS-718 Nov. 2001

RESEARCH REPORT
NIFS Series

TOKI, JAPAN

Interaction of Cover and Target with Xenon Gas in the IFE-Reaction Chamber

Boris V. KUTEEV

State Technical University, St. Petersburg 195251, RUSSIA
National Institute for Fusion Science, Toki, Gifu 509-5292, JAPAN

e-mail: kuteev@phtf.stu.neva.ru

Keywords: target, cover, drag force, gas dynamics, heat transport.

Abstract:
Interaction of a direct drive target and a cover, which is shielding the target against gas particle and heat flows in the reaction chamber of the Inertial Confinement Reactor, is considered. The cover is produced from solid gas –deuterium, neon of xenon. It is shown that at the SOMBRERO parameters the xenon cover with 5.6-mm size significantly reduces the heat flows onto the 4-mm target. The gas drag produces the deceleration of the target much larger than that for the cover due to large mass difference between them. The distance between the target and the cover is about 15 mm at the explosion point, which is sufficient for normal irradiation of the target by laser beams. Protection of the target against the wall radiation is necessary during the flight. Along with creation of reflecting layers over the target surface ablating layers from solid hydrogen or neon seem to be a solution.

1 Introduction

According to the scenario of Inertial Fusion Energy (IFE) power plant operation, cryogenic targets should be delivered into the reaction chamber with frequency about 5 Hz and velocity of a few hundred meter per second [1,2]. The problem of direct drive target interaction with gas and radiation in the reactor chamber as well as motion parameters of the target and transporting sabot were recently considered in Ref. [3,4]. It was concluded that both radiation and gas heat transfer are the factors significantly affecting the target temperature and design parameters of the target and the reactor chamber. Particularly, the target surface is to be reflecting at a rather high level (0.98) to prevent excess heating by radiation or is to be coated by a protecting layer or the sabot separation should be delayed to the last stage of delivery being produced right before irradiation. The gas heating "far outweighs" that caused by the radiation heating. That is, "gas filled reaction chamber must have gas pressure and wall temperatures less than previously assumed... in current direct drive target designs".

Several new ideas about the target transportation and protection against the radiation and gas flows were formulated in Ref. [5]. For the target protection it was proposed to use a cover moving ahead the target and reducing the gas and radiation load onto the direct drive target. A schematic of such approach is shown in Fig. 1. For evaluation of the approach it is necessary to consider quantitatively interaction of such a system with gas and radiation in the reaction chamber.

Below the problem of gasdynamic interaction of the cover and target with hot gas and radiation in the chamber of IFE reactor is considered.

2 Problem Formulation

2.1. Reactor parameters

Let us consider the interaction of a body with the gas and radiation in a SOMBRERO like reactor [3].
The radius of reaction chamber is 500 cm (really 650 cm).
The wall temperature is 1500 C, or 1773 K.
The wall radiation is 12 W/cm^2. (really 54 W/ cm^2).

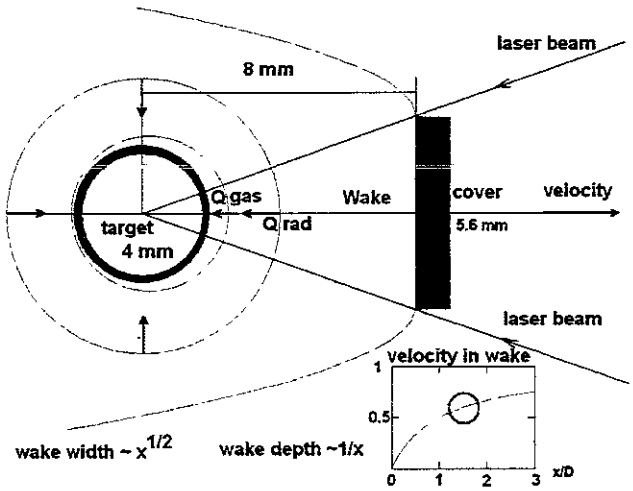

Figure 1: Schematic diagram of the cover and target motion and positioning in the reaction chamber of IFE power plant. The target is located at the destination point in the camber center. The optimal distance between the target and the cover 80 mm equal to 1.43 of the cover diameter allows the laser beams to irradiate the target.

The xenon gas pressure is 0.5 Torr specified at 1773 K (really specified at 300 K). This means 3 Torr at (1800 K). We should assume something about the gas pressure in the transporting pipe system. Let it be the same pressure of Xe as in the reactor. Another option as vacuum up to the chamber should be considered as well. The temperature of the guide tube is 600 K.

2.2. Target and cover parameters

The cover is made from solid Xe. We assume its temperature 4.2 K at the entrance into the reaction chamber. The cover has cylinder shape being 0.56 cm in diameter and of 0.1-cm thickness. The cover mass is then 87 mg.

The target is a sphere of 4 mm diameter. We assume that the target is made using LPI technology (see [5] and references in it) and its temperature is 4.2 K. The size is very close to that (3.96 mm) considered in Ref. [6]. No special coating by gold is supposed in our case, so that zero reflection for the wall radiation by target surface is assumed. The target mass is 5 mg.

Both the cover and target have initial velocity v=250 m/s, which corresponds to 20 ms flight time in the chamber with 500-cm radius. Both the cover and target rotate around the injection axis with the angular frequency $\Omega = 2 \cdot \pi \cdot v/L$ for the trajectory stabilization [3]. The rotation is produced by one-loop grooves in the barrel wall. Here L =25 cm is the barrel length.

2.3. The critical issues of the problem

Answers to the following questions are desirable to get as a result of the analysis.

How large is the cover and target deceleration by xenon gas during the flight in the chamber?

How large is the cover and target heating and shielding factors for the radiation and gas heat flow produced by the cover for the target?

What is an optimal positioning the target relative to the cover at the shot moment?

What is the optimal velocity difference between the cover and target at the entrance of the chamber?

How significant is the impact of rotation on the trajectory stabilization?

Similar problems for a solitary target have been analyzed in Ref. [4] using the Direct Simulation Monte Carlo (DSMC) approach [7]. The simulations were carried out using program [8]. This program gives the drag and heat flow coefficients for various values of Mach and Knudsen numbers as well as different boundary conditions on the body surface. It is convenient for evaluations, especially for the intermediate case between hydrodynamic and free molecule regimes. This is the case for the target gas interaction with gas during flight, as will be clear soon.

A part of the analysis can be carried out also in analytic or semi-analytic form using results of numerous studies of gas flows interaction with bodies. Those will be mentioned sequentially below when their results will be used.

2.3. Dimensionless parameters of the problem

The problem of gas-body interaction is the main problem of boundary-layer theory [8]. The dimension analysis shows that there are several dimensionless parameters, which define dependencies of any value of the problem. Those are

The Mach number

$$M = u/a \quad (1)$$

The Knudsen number

$$Kn = \lambda/R \quad (2)$$

The Reynolds number

$$Re = (u \cdot R)/\nu \quad (3)$$

Here u is the velocity of the body, a is the sound speed in gas

$$a = (\gamma * Tg/Mg)^{0.5}, \quad (4)$$

λ is the mean free pass, R is the body radius, ν is the kinematic viscosity, γ is the specific heat ratio equal to 5/3 for xenon, Mg is the gas mass, Tg is the gas temperature.

Table 1 shows the values of these parameters for the cover and target.

Table 1.

Body	*M*	*Kn*	*Re*	Gas parameters		
cover	0.579	0 234	5.83	Tg=1800 K	P=0.5 Torr	V=250 m/s
0.56 cm		0.039	35	Tg=1800	P=3.0	
	1 407	0.0246	116 55	Tg=300	P=0.5	
		0.0041	699	Tg=300	P=3.0	
target	0.579	0.327	4.16	Tg=1800	P=0.5	
0.4 cm		0.055	25	Tg=1800	P=3.0	
	1.407	0.0345	83.25	Tg=300	P=0.5	
		0.0057	500	Tg=300	P=3.0	

One can see from Table 1 that during the flight in guide tube the regime will be supersonic M>1, while inside the reaction chamber the regime will likely be transonic or very close to the transition if the guide tube will be heated by 300 C or higher.

The Knudsen number for the conditions is small enough. This means that Stokes solutions are admissible for the drag and heat transfer evaluations. However, inside the camber chamber the regime deviates to the free molecular regime, so corrections for the drag and heat transport to Stokes solutions are necessary.

In the whole operation domain, the Reynolds number is smaller than 2000. This means that laminar flow solutions are probably valid everywhere [8].

The Prandtl parameter is also necessary for evaluation the gas characteristics (0.7 for air) do to difference of temperatures of the gas and body and compression effects

$$P=\nu/a=(\mu c_p)/k \qquad (5)$$

Approximately,

$$Pr=\frac{\gamma}{1+\frac{9}{4}\frac{Rg}{c_V}} \qquad (6)$$

Here ν is the kinematic viscosity, μ is the dynamic viscosity, c_p is the specific heat at constant pressure and k is the thermal conductivity, γ is the ratio c_p/c_v of the specific heats and Rg=8.31 J/mol·K is the gas universal constant. For xenon, the Prandtl number P is equal to 0.654 (0.64 from the expression (6)). For Deuterium Pr=0.695 (0.73 from the upper expression). The value slowly varies with the temperature (See Fig. 2 for xenon).

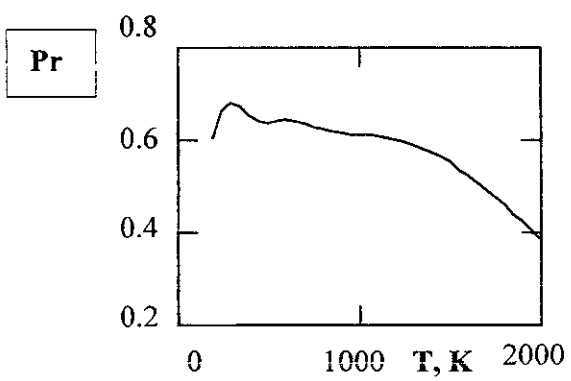

Figure 2: The Prandtl number for xenon versus gas temperature.

3 Effect of Rotation on the Motion

The effect of disk/sphere rotation on the boundary layer is characterized by the parameter $\Omega r/u$, the value is equal to 0.07 for our conditions. The parameter is very small to be significant for the modifications of the boundary layer (see [8] p. 244). Therefore, we neglect by rotation effect on the drag and heat transport.

Precession of the target and cover during flight is a possible source of errors in the tracking system [3]. However, even the momentum equal to a product of the drag-force and the cover/target radius gives the upper extreme of precession frequency

$$\Omega_{prec}=\frac{F_{drag}}{\Omega\times M\times r}, \qquad (7)$$

still laying in the Hz range. For such a low precession frequency we can neglect its effect on the flight parameters.

4 Drag Evaluations for the Solitary Cover and Target

Deceleration of the cover and target solitary moving in the reaction chamber can be evaluated immediately using expressions for drag coefficient given in Ref. [8].

According to Oseen theory valid till R_D<5, the drag is defined by expressions

$$C_D=\frac{24}{R_D}\left(1+\frac{3}{16}R_D\right),$$
$$R_D=\frac{2\cdot u\cdot R}{v_\infty} \qquad (8)$$
$$Drag=\frac{1}{2}C_D\cdot\pi\cdot R^2\cdot\rho\cdot v_\infty$$

For R_D=11.66 (cover, Tg=1800 K, P=0.5 Torr) C_D=6.45 and $Drag$=327 din. The experimental drag for these conditions is C_D^{exp}=4 (see fig.1.5 of Ref. [8]).

On the other hand, the evaluation can be made using results of analytic solution for the free molecular regime [11] and the corresponding experimental dependence on Knudsen number obtained by Millikan [12]. For equal temperatures of gas and body as well as diffusion molecule reflection (σ=1), the drag force is defined by

$$Drag = \zeta \cdot u_\infty$$

$$\zeta_{anal} = \frac{\pi \cdot m \cdot n \cdot u_\infty \cdot R^2}{2} f(s)$$

$$f(s) = \frac{1}{s^2}\left[\frac{4s^4+4s^2+1}{2s} erf(s) + \frac{2s^2+1}{\sqrt{\pi}} e^{-s^2}\right] + \frac{2}{3}\frac{\sigma}{s}\sqrt{\pi}$$

$$s = \frac{u_\infty}{(2kT/m)^{1/2}} \qquad (9)$$

when n is the molecular number density, m is the mass of a single gas molecule and s is the speed ratio.

For the cover in free molecular regime (Kn>>1), the coefficient C_D=f(s) is equal to 9.1 and the drag force is $Drag$=454 din. According to the Knudsen number correction [12], the drag coefficient should be 0.274. That is, C_D=2.49.

Experiments with disks and simulations by DSMC performed in Ref. [13] give very close to this value C_D=2.5 at T_w/T_o close to zero, which corresponds to our situation. Therefore, we'll use this value for the following deceleration analysis.

Let us evaluate the distance, which the cover passes during 20 ms flight. Deviation from 500 cm will give us the estimation of the deceleration effect.
The equation of motion

$$L_{cov/targ} = v_\infty \cdot t - \frac{Drag}{2 \cdot M_{cov/targ}} \cdot t^2 \qquad (10)$$

gives L_{cov}=499.714 cm for the cover and L_{targ}=497.466 cm for the target. This means that due to drag force the solitary moving cover and target would get a pretty nice separation being the order of 4 cover diameters (2.248 cm). Really, due to shielding effect the separation will be less and we shall return to this issue later in Section 7.

Obviously, the separation distance will be about 6 times larger for the gas pressure 3 Torr being assumed.

5 Heat Transport for the Solitary Cover and Target

5.1. Heating power

In free molecular regime, the heat flow distribution over a sphere can be evaluated following Probstain [14]

$$a_e = \frac{E_i - E_r}{E_i - E_b} \qquad (11)$$

when
E_i=1773 K is the incident particle temperature,

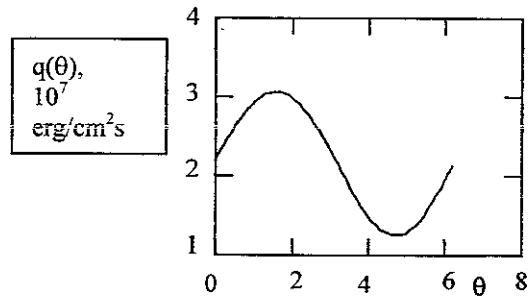

Figure 3: Angular distribution of the heat flux q in free molecular regime for s=0.525 and a_e=1. Maximal heat flow located near the forward stagnation point is three times higher than that near the backward stagnation point.

E_r=20 K is the reflected particle temperature,
E_b=20 K is the border temperature.
For our conditions the coefficient a_e is close to unity.
The heat flux q is defined via the speed ratio s by the expression

$$q(\theta) = -a_e \cdot P_g \left(\frac{RB \cdot E_i}{2 \cdot \pi}\right)^{1/2} \times$$
$$\left[\left[s^2 + \frac{\gamma}{\gamma-1} - \frac{\gamma+1}{2\cdot(\gamma-1)}\frac{E_b}{E_i}\right] \cdot exp\left[-(s \cdot sin(\theta))^2\right] + \right.$$
$$\left. \pi^{1/2} \cdot s \cdot sin(\theta) \cdot (1 + erf(s \cdot sin(\theta))) - \frac{1}{2} exp\left(-(s \cdot sin(\theta))^2\right)\right] \qquad (12)$$

Here θ=π/2 corresponds to the falling flux. The distribution of the heat flux over the sphere surface is shown in Fig. 3.

The average flux about $2.8 \cdot 10^7$ erg/cm^2·s is expected. The flux is distributed around the surface non-uniformly being three times higher from the gas flow direction. The average power transported onto the sphere with the cover radius will be $6.7 \cdot 10^6$ erg/s or 0.67 W.

A close to that heat flux can be evaluated using simple formula of convective heat transfer

$$q = n \cdot v_\infty \left(\frac{3}{2}kT + H_{subl} + \frac{m \cdot v_\infty^2}{2}\right) \qquad (13)$$

This expression gives for the average flux $2.5 \cdot 10^7$ erg/cm^2*s (for H_{subl}=$2.48*10^{-13}$ erg/atom). The sublimation and melting energy for xenon should be taken into account in a case of condensation at the cryogenic surface.

A standard approach of heat transport evaluation based on calculations of the Nusselt number [15] gives the following results:

$$Nu_D = 2 + \left(0.4 \cdot Re_D^{1/2} + 0.06 \cdot Re_D^{2/3}\right) \cdot Pr^{0.4} \cdot \left(\frac{\mu_\infty}{\mu_s}\right)^{1/4} \quad (14)$$

when all properties except μ_s (dynamic viscosity at the body surface) should be evaluated at T_∞. Figure 4 shows variation of the Nusselt number with the wall temperature in range 200-1500 K. The convective part is comparable with the diffusive one. The total power onto the sphere is then

$$W_{gas} = Nu_D \cdot \frac{\lambda}{D} \cdot \pi \cdot D^2 \cdot (T_\infty - T_s) \quad (15)$$

being equal to 3.5 W. This value is significantly higher than the rough evaluations presented above. It is possible that the standard formula is not applicable in our property range. With average heat conductivity at T=200 K the formula gives almost the same result 0.7 W as those mentioned above.

The last cross-checking can be made using the experimental results of Legge et al. [13]. They give evaluation of the heat flow onto the disk using the Stanton number St=0.369 for Kn=0.2.

$$W_{gas} = St \cdot m \cdot n \cdot v_\infty \cdot c_p \cdot \left(T_\infty \cdot \frac{2 \cdot \gamma}{\gamma + 1} - T_s\right) \cdot \pi \cdot R^2 \quad (16)$$

This expression gives the heat power equal to 0.52 W. That is, all mentioned above estimations agree with each other at the accuracy of 30 %.

We'll use the value 0.67 W in the cover heating evaluations. Similarly, for the target we use 0.4 W.

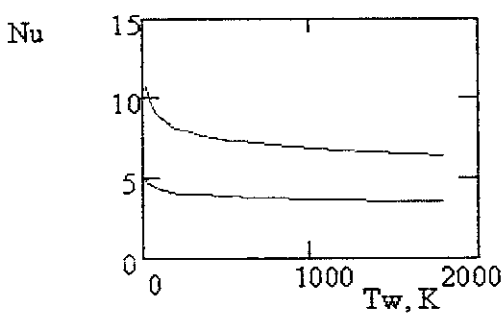

Figure 4: The average Nusselt number variation with the wall temperature. The blue curve corresponds to Re=100. The red one corresponds to our conditions Re=11.5.

5.2. The cover temperature variation in flight

The heating power for the cover can be assumed fixed during the flight. Meanwhile, the specific heat of solid xenon significantly varies in the temperature range 4-200 K [16]. The specific heat dependence is presented in Fig. 5 for xenon.

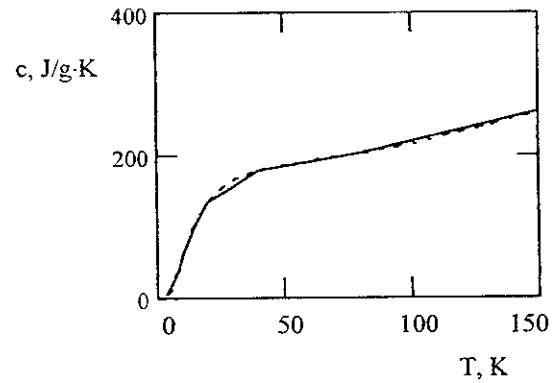

Figure 5: Heat capacity for solid xenon (in J/g·K). Experiment –red line. Approximation – blue line.

Corresponding to that specific heat variation, the cover temperature dependence described by

$$\frac{dT}{dt} = \frac{Q_{rad} \cdot \left(2 \cdot \pi \cdot R_{cov}^2 + 2 \cdot \pi \cdot R_{cov} \cdot l_{cov}\right) + W_{gas}}{k_{Xe}(T) \cdot M_{cov}} \quad (17)$$

is shown in Fig. 6.

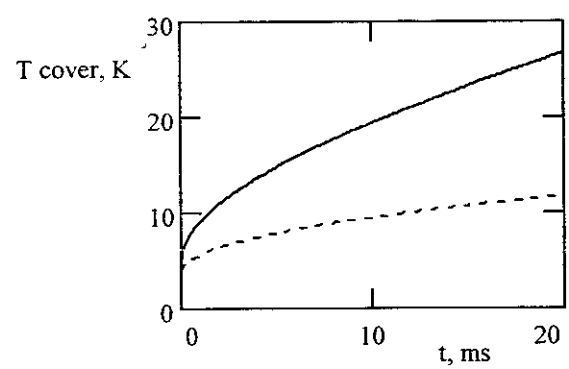

Figure: 6. The cover temperature variation in flight. Red line accounts for a joint effect of 12 W/cm^2 radiation and the gas heat transfer (0.5 Torr, 1773 K, 250 m/s). Blue curve describes the gas heat transfer only.

It is seen that the gas effect is not so large, the temperature increases only by 6-7 K. However totally including radiation heating, the temperature increase up to 30 K is expected. The temperature is still less than the melting point for xenon (161 K). That is, the cover will be solid at any moment of the flight. At the radiation level of 54 W/cm^2, the sublimation will take place, eventually. The saturated pressure for xenon is equal to 1 Torr at 103 K. This means that the sublimation will save the solid structure of the cover even at a higher level of heat transfer.

Due to a significantly smaller mass (5mg), one would expect that the target heating would be higher. However, owing to a fast growth of the specific heat for hydrogen isotopes at the temperature above 10 K (see Fig. 7), the target temperature remains in a reasonable domain even without the reflecting cover. It should be noticed that the specific heat for deuterium is no more than 20% higher than the hydrogen one. So, we use the hydrogen properties in calculations because those are given for a wider temperature range.

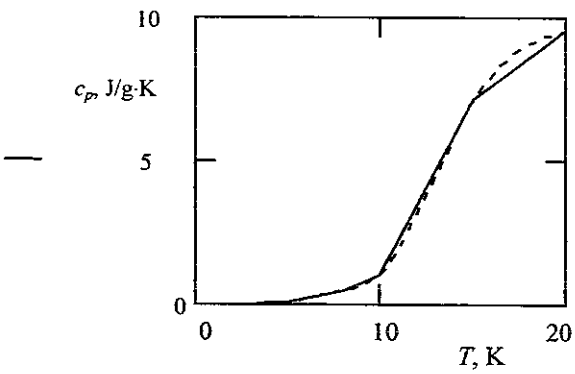

Figure: 7: Specific heat for hydrogen at the constant pressure. Read line is experiment. Blue line is approximation.

Figure 8 shows the target temperature increase in a case of irradiated target (12 W/cm^2) without and with the reflecting shell. Even if the golden protecting layer provides 99% -reflection, the temperature will rise about 2K. Figure 9 shows the effect of joint radiation and gas convection as well as separate gas convection effect. This is an average temperature. For the gas flow it is necessary to account for the angular distribution, which will make the temperature field non-uniform.

The distribution over the surface of spherical target can be imagined via Fig. 7.9 in Ref. [15]. The lowest power density is expected nearby the separation point (80 grad). The difference with the stagnation point is about 3 times.

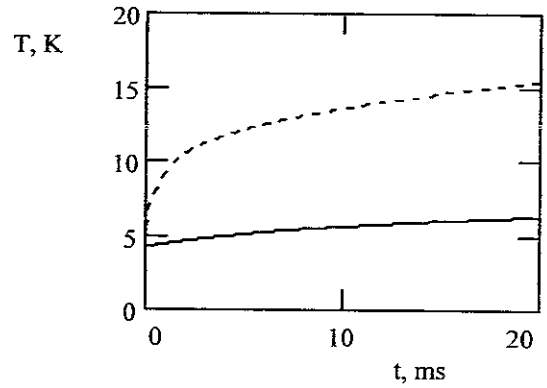

Figure 8: The target temperature variation under irradiation by 12 W/cm^2 power only. Blue curve corresponds to a no reflecting shell. Red curve is for reflecting shell (99%).

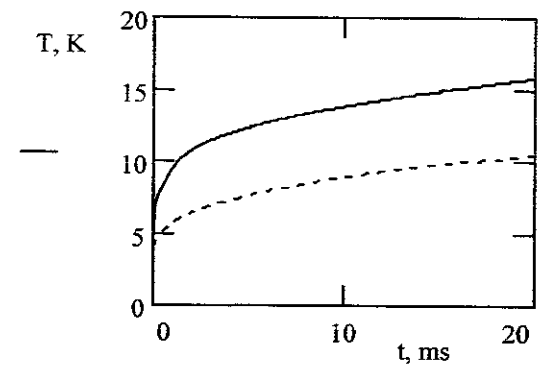

Figure 9: The target temperature variation under irradiation by 12 W/cm2 and uniform gas heat load (xenon, 1773 K, 0.5 Torr, 250 m/s). The red curve corresponds to joint effect of the radiation and gas convection. The blue one accounts for the gas convection effect only.

6 Wake Parameters

The velocity distribution in a laminar circular wake behind the cover can be described by the formula [8] p.235

$$u_1(x,y) = U_\infty \times \frac{\pi c_D}{32}\left(\frac{2\cdot R}{x} RD\right) exp(-\eta^2) \qquad (17)$$

$$\eta = \frac{y}{2}\cdot\sqrt{\frac{v_\infty}{\nu\cdot x}}$$

The central velocity dependence is shown in Fig. 1. It is seen that, if the target (blue circle) is in the wake, the velocity of the contacting it flow is reduced at least by a factor of two or

even higher in average. A two-dimensional plot of the velocity distribution in the wake is illustrated by Fig. 10. Since the Prandtl number is close to unity, the curves of constant velocity are identical with the isotherms ([8] p.330). So, we can expect the corresponding reduction of the heat flux also.

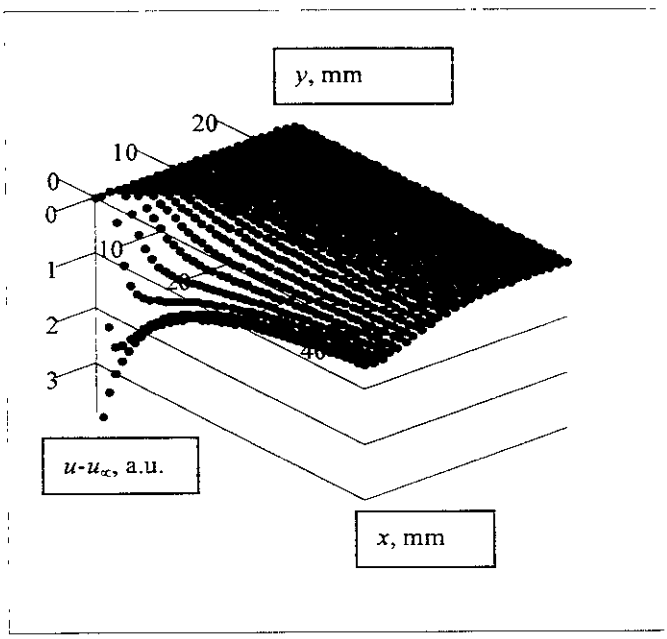

Figure 10: Velocity distribution in the wake.

Totally, both velocity and temperature drops in the wake yield at least four times reduction of the heat transfer onto the target. A more detailed information can be obtained using DSMC technique.

7 Drag Evaluations for the System of Cover and Target

Analyzing joint motion of the cover and target one should take into account additional effects. Several authors [17-21] analyzed the problem of two-body drag. Both objects have different drag force compared with solely motion case. For a target, the drag force has the form [21]

$$Drag = -\frac{3 \cdot k_B \cdot T \cdot n_o \cdot a^2 \cdot M}{2 \cdot \pi} F_1 \cdot \bar{k} =$$

$$-\frac{3}{4} \cdot a^2 \cdot n_o \cdot u \cdot \left(\frac{m_g \cdot k_B \cdot T}{2 \cdot \pi} \right)^{1/2} \cdot F_1 \cdot \bar{k} \qquad (18)$$

$$F_1 = F_{1o} + F_{1p}$$

$$F_{1o} = 8 \cdot \pi \cdot (8 + \pi)/9$$

Here F_{1o} and F_{1p} are dimensionless drag coefficients. F_{1o} is the drag on target in the limit of infinite separation.

Approximately, the drag reduction is proportional to the solid angle at which the target sees the cover. So, the effect reduces as the inverse square of the distance between these two bodies

For two equal spheres Ref. [21] gives in free molecular regime the following expression for F_{1p}

$$F_{1p} = -\frac{21.28}{\chi^2} \qquad (19)$$

when χ is the dimensionless distance measured in the sphere radii

The drag reduction about 15 % is expected for two spheres. In our case we can expect a higher reduction, may be as much as 30% caused by cylindrical shape of the cover and its diameter larger than target one. In the region nearby χ=2-3 (contact conditions) the value of F_{1p} varies rather slowly (see Fig. 4 of Ref. [21]). So, we can evaluate the drag reduction effect as proportional decrease of the distance between the cover and target from 22 mm (initially evaluated) to 15 mm. This value is acceptable for irradiation the target by the laser beams.

8 Condensation and Ablation Effects

During flight both cover and target have the temperature significantly lower than the surrounding gas.

On the one hand, we can expect condensation of the xenon at the cryogenic surfaces of cover and target. According to Eisenshtadt [22] the condensation of high-energy particles depends on the ratio of sublimation and gas thermal energies. Figure 11 shows the accommodation coefficient as function of this ration. In case of xenon the sublimation energy is about the thermal inside the chamber, so less than 10% of impinging particles will accommodate to the surface. However, due to a very strong dependence on the temperature and reduction of the temperature nearby the surface due to heat conductivity effects, the accommodation can be much higher than evaluated at the infinite temperature, may be close to 1.

Table 2

Gas	Density, g/cm^3	Sublimation energy, eV/atom *)meV/mol	Surface temperature, K	Surface density, 10^{18}/cm^3	Surface velocity, 10^3 cm/s	Erosion speed, μ/c
Helium	0.122	0.86	1.53	34.17	7.32	33650
Hydrogen	0.708	9.3 *)	9.49	1.11	25.8	3330
Deuterium	0.165	13 *)	12.22	1.01	20.7	2080
Neon	2.205	19	16.47	1.22	10.75	490
Argon	1.4	80	54.8	0.26	13.8	420
Xenon	3.52	155	108	0.17	10.75	290

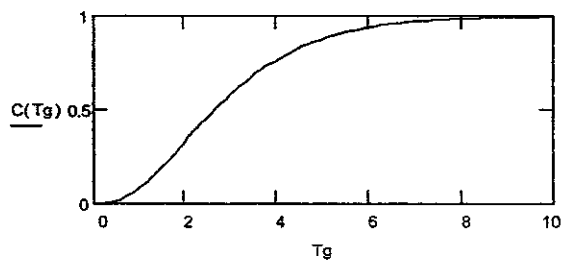

Figure 11: The accommodation coefficient for a gas versus the ratio of sublimation to gas thermal energies according to [22]. Our case corresponds to Tg=1 and accommodation coefficient 0.08.

In this case, the gas flow in the wake will change. Nearby the cover a back flow onto the surface is expected. The heat conductivity will also affect the heat transfer onto the target making the heat flows smaller. However, quantitatively such a problem still needs additional analysis.

On the other hand, ablation of the cover and target can take place due heat transport by radiation and gas. With this ablation, the problem becomes even more complicated. Ablation particle flux for the xenon cover under the radiation flux 12 W/cm^2 can be as large as $4.8 \cdot 10^{20}$ atom/cm^2·s

This flow at a sonic speed and the temperature of 110 K can produce a cloud with the density about ~ 10^{17} atom/cm^3. Table 2 shows erosion characteristics for different gases in solid state at radiation flux 12 W/m^2. The surface temperature was determined assuming saturation pressure for gas and outward radial velocity at the surface equal to ¼ of the local sound velocity.

Dividing the erosion speed by 50 (1/20 ms), it is easy to evaluate the eroded thickness for different gases during the flight time. For example, xenon will loose about 6 microns, while deuterium about 40 μ.

For the reactor chamber conditions, the gas density is $3 \cdot 10^{15}$, that is two orders less than the cloud density. Two significant conclusions can be made comparing the cloud density nearby the cover and target (if covered by protecting layer) with the chamber gas density.

The first one is that in rigorous analysis the boundary layer should be considered as binary with injection.

The second one is that owing to a low gas temperature close to the cover and target, the kinematic viscosity and heat conductivity of the media around the cover and target will be drastically reduced. This means that the problem differs greatly from that considered in contemporary references. Particularly, the wake will likely be deeper and longer than it is presented here in Fig. 10. So, the estimations presented here upward describe only qualitative features of the phenomenon.

It should be noticed that hot xenon atoms enable to penetrate through the hydrogen/deuterium clouds with density up to 10^{18} cm^{-3}. Thus, the gas heating during expansion will determine the cloud structure similar to case of pellet ablation in high temperature plasma [23]. The neutral gas shielding effect is possible in these conditions, which should be evaluated quantitatively as well.

The surface evaporation instead of gradual heating at average specific heat that evaluated here in Session 5 might take place in experimental conditions considered. Figure 12 drawn according to data presented in Ref. [24] shows dependencies of the thermal conductivity versus temperature for solid and liquid hydrogen, neon and xenon. Actually, the heat conductivity of solid xenon and hydrogen is about 10 mW/cm·K. This means that at the radiation energy flux 12 W/cm^2, the temperature drop at 1 mm of solid gas will be about 120 K, which is sufficient for surface ablation with a slight volume heating. Meanwhile, for a thin hydrogen layer in target (0.2 mm) with increased heat conductivity (by a factor of 100 at low temperatures of about 4 K) the average specific heat is permissible to use.

9 Conclusions

It is clear from the analysis presented that the concept of protection the direct drive target in the reaction chamber by a cover moving ahead it can be considered as a possible way of solving the target delivery problem. The concept gives a

chance to save the design parameters of the reactor, particularly the gas pressure and wall temperature.

The minimal distance between the cover and target 8 mm for 5.6 mm cover and 4 mm target is provided naturally by larger acceleration of the target due to significantly smaller mass (at Tg=1800 and Pg=0.5 Torr). This occurs even if no difference between the cover and target velocities exists at the chamber inlet. The evaluated separation distance at the shot moment equal to 15-16 mm seems reasonable both for the laser beams propagation and target protection by wake effect

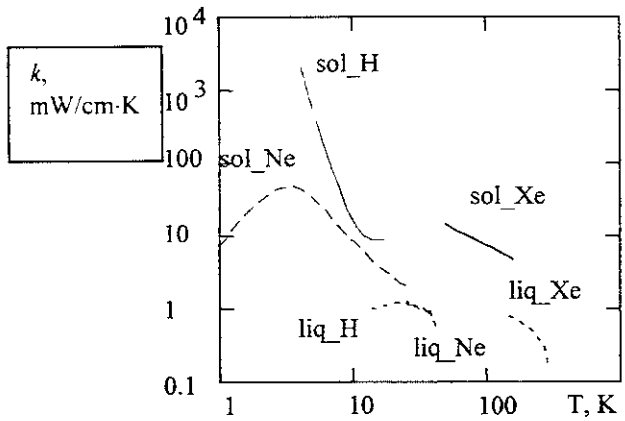

Figure 12: Thermal conductivity for solid and liquid Hydrogen, Neon and Xenon (in mW/cm·K).

The main heating of the cover and target is produced by the radiation (12 W/cm^2). The heat flow transported by gas is by a factor of 10 less. Meanwhile, the gas heat flow becomes determining in a case of the reflecting target. For such a type of target, the cover effect might be most significant.

Quantitatively, the shielding effect is of the order of 4 according to these estimations. It is possible that with intensively sublimating cover its efficiency can be improved both due to the gas cooling and the viscosity reduction.

Evaluations of gas sublimation under irradiation show a natural mechanism of target protection by a sublimating layer that evaporates during the flight to the ignition point. A target design and technology development for such layer coating should be considered as an alternative to reflecting layers.

The effect of the target rotation on the target-gas interaction is negligible. Nevertheless, the rotation in the barrel will stabilize the trajectory like in a rifle and seems a necessary factor for the injection system.

The analysis presented does not include gas injection effects on the wake formation and drag. This factor should be obviously taken into account in further development of the concept.

Acknowledgements

The author is grateful to Prof. S. Sudo and Prof. L. D. Tsendin for their attention to the work and fruitful discussions.

References

1. W.R. Meier, "Osiris and SOMBRERO Inertial Fusion Power Plant Design-summary, conclusions and recommendations", Fusion Eng. Des. **25** (1994) 145.
2. R.W. Moir, et al., Fusion Technol. "HYLIFE-II: A Molten-Salt Inertial Fusion Energy Power Plant Design-Final Report", **25** (1994) 5.
3. R.W. Petzoldt, "IFE Target Injection and Tracking Experiment", Fusion Technol. **34** (1998) 831-839.
4 D.T. Goodin, N.V. Elexander, C.R. Gibson, et al., "Developing Target Injection and Tracking for Inertial Fusion Energy Power Plant", Nuclear Fusion, **41** (2001) 527-535.
5. I.E.Osipov, et al., "A Device for Cryotarget Rep-Rate Delivery in IFE Target Chamber", IFSA-2001 (Kyoto) report number IFSA0908.
6. S.E. Bodner, et al. "High –Gain Direct-Drive Target Design for Laser Fusion", Phys. Plasmas, (in press).
7. G.A. Bird, "Molecular Gas Dynamics and the Direct Simulations of Gas Flows", Oxford University Press, Oxford (1994).
8. H. Schlichting, "Boundary-Layer Theory", McGraw-Hill, 1979.
9. M.G. Rogers, G.N. Lance, "The rotationally symmetric flow of a viscous fluid in presence of an infinite rotating disk", JFM 7, 617-631 (1960).
10. E.M. Sparrow, J.L. Gregg. "Mass transfer, flow and heat transfer about a rotating disk", Transactions ASME, J. Heat Transfer, **82**, 294-302 (1960).
11. S.A. Schaaf, in Fluid Dynamics II. Handbuch der Physik, Gruppe 3, Band 8, Teil 2, edited by S. Fluegge and C. Truesdell (Springer, Berlin, 1963), pp. 591-624.
12. R. Millikan, "The general law of fall of a small spherical body through a gas, and its bearing upon the nature of molecular reflection from surfaces", Phys. Rev. **22** (1923) 1.
13. H. Legge, K. Nambu, S. Igarashi, "Force and Heat Transfer on a Disk in Rarefied Flow " Rarefied Gas Dynamics, ed. by A.E. Beylich. Proc. 17-th Int. Symp. On RGD, 1990, Aachen, Germany, p.679.
14. R.F. Probstain, "Aerodinamics of Rarefied Gases" in "International Series on Aeronautical and Space Flight" Rarefied Gas Dynamics, Proceedings of the First International Symposium held at Nice. Ed. F.M. Devienne. Pergamon Press. 1960. p. 269.
15. F.N. Incropera, D. P. DeWitt, "Fundamentals of Heat and Mass Transfer", J.Wiley and Sons, N.Y., 1998, p. 339.

16. Handbook. "Physical values", ed. I.S. Grigoriev and E.Z. Meilikhov, Moscow, Energoatomizdat, 1991.
17. B. Dahneke, P. Chan, "Monte-Carlo Calculations of the Free-Molecular Drag on Chains of Uniform Spheres" in Rarefied Gas Dynamics: Progress in Astronautics and Aeronautics, Edoted by S.S. Fisher (American Institute of Astronautics and Aeronautics) p.1031-1039, (1980).
18. M.H. Peters "Nonequilibrium molecular dynamics simulation of free-molecilar gas flows in complex geometries with application to Brownian motion of aggregate aerosols. Phys. Rev. E. **50** (1994) 4609-4617.
19. M.H. Peters, "Analytic (perturbation) solution to the problem os free-molecule gas flows in two-body systems: Results for flows over two unequal-size cylinders.
20. M.N. Kogan, I.N. Bobrov, C. Cergiani, A. Frezzotti. "Interaction of evaporating and condensing particles in free-molecular regime". Phys. Fluids, 7 (1995) 1775-1781.
21. A. Gophinath, D.L. Koch, "Hydrodynamic interactions between two equal spheres in highly rarefied gas", Phys. Fluids, **11** (1999) 2772-2787.
22. M.M. Eisenshtadt, " Condensation of Gases during Cryopumping-The Effect of Surface Temperature on the Critical Energy for trapping", Int. J. Vac. Sci. and Tech. 7 (1970) 479-484.
23. B.V. Kuteev, "Pellet Technoligies for Fusion Reactors", J Techn. Phys., **69** (9), (1999) 63.
24. Thermal Properties of Matter. Vol. 3. Thermal Conductivity. Nonmetallic Liquids and Gases, Edited by Y.S. Touloukian, P.E. Lisey and S.C. Saxena, IFI/Plenum, NY-Washington, 1970.

Recent Issues of NIFS Series

NIFS-693 W Pei, R Horiuchi and T Sato
Long Time Scale Evolution of Collisionless Driven Reconnection in a Two-Dimensional Open System Apr 2001

NIFS-694 L N Vyacheslavov, K Tanaka, K Kawahata,
CO2 Laser Diagnostics for Measurements of the Plasma Density Profile and Plasma Density Fluctuations on LHD Apr 2001

NIFS-695 T Ohkawa,
Spin Dependent Transport in Magnetically Confined Plasma May 2001

NIFS-696 M Yokoyama, K Ida, H Sanuki, K Itoh, K Narihara, K Tanaka, K Kawahata, N Ohyabu and LHD experimental group
Analysis of Radial Electric Field in LHD towards Improved Confinement May 2001

NIFS-697 M Yokoyama, K Itoh, S Okamura, K Matsuoka, S -I Itoh,
Maximum-J Capability in a Quasi-Axisymmetric Stellarator May 2001

NIFS-698 S-I Itoh and K Itoh,
Transition in Multiple-scale-lengths Turbulence in Plasmas May 2001

NIFS-699 K Ohi, H. Naitou, Y Tauchi, O Fukumasa,
Bifurcation in Asymmetric Plasma Divided by a Magnetic Filter May 2001

NIFS-700 H Miura, T Hayashi and T Sato,
Nonlinear Simulation of Resistive Ballooning Modes in Large Helical Device June 2001

NIFS-701 G Kawahara and S Kida,
A Periodic Motion Embedded in Plane Couette Turbulence June 2001

NIFS-702 K Ohkubo,
Hybrid Modes in a Square Corrugated Waveguide June 2001

NIFS-703 S -I Itoh and K Itoh,
Statistical Theory and Transition in Multiple-scale-lengths Turbulence in Plasmas June 2001

NIFS-704 S Toda and K Itoh,
Theoretical Study of Structure of Electric Field in Helical Toroidal Plasmas June 2001

NIFS-705 K Itoh and S-I Itoh,
Geometry Changes Transient Transport in Plasmas June 2001

NIFS-706 M Tanaka and A Yu Grosberg
Electrophoresis of Charge Inverted Macroion Complex Molecular Dynamics Study July 2001

NIFS-707 T-H Watanave, H Sugama and T Sato
A Nondissipative Simulation Method for the Drift Kinetic Equation July 2001

NIFS-708 N Ishihara and S. Kida,
Dynamo Mechanism in a Rotating Spherical Shell Competition between Magnetic Field and Convection Vortices July 2001

NIFS-709 LHD Experimental Group,
Contributions to 28th European Physical Society Conference on Controlled Fusion and Plasma Physics (Madeira Tecnopolo, Funchal, Portugal, 18-22 June 2001) from LHD Experiment July 2001

NIFS-710 V Yu Sergeev, R.K Janev, M.J Rakovic, S Zou, N Tamura, K V Khlopenkov and S. Sudo
Optimization of the Visible CXRS Measurements of TESPEL Diagnostics in LHD, Aug 2001

NIFS-711 M Bacal, M Nishiura, M Sasao, M Wada, M Hamabe, H Yamaoka,
Effect of Argon Additive in Negative Hydrogen Ion Sources Aug 2001

NIFS-712 K Saito, R Kumazawa, T Mutoh, T Seki, T Watari, T Yamamoto, Y Torii, N Takeuchi C Zhang, Y Zhao, A Fukuyama, F Shimpo, G Nomura, M Yokota, A Kato M Sasao, M. Isobe, A V Krasilnikov, T Ozaki, M Osakabe, K Narihara, Y Nagayama, S Inagaki, K Itoh T Ido, S Morita, K. Ohkubo M. Sato, S Kubo, T Shimozuma, H Idei, Y Yoshimura, T Notake, O. Kaneko, Y Takeiri, Y Oka, K Tsumori, K Ikeda, A Komori H Yamada, H Funaba, K Y Watanabe, S Sakakibara, R Sakamoto, J. Miyazawa, K Tanaka, B J Peterson, N Ashikawa, S Murakami, T Minami, M Shoji, S Ohdachi, S Yamamoto, H. Suzuki, K Kawahata, M Emoto, H Nakanishi, N Inoue, N. Ohyabu, Y Nakamura, S Masuzaki, S. Muto, K Sato, T Morisaki, M Yokoyama, T Watanabe, M Goto, I Yamada, K Ida, T Tokuzawa, N Noda, K Toi, S Yamaguchi, K Akaishi, A Sagara, K Nishimura, K Yamazaki, S Sudo, Y Hamada, O Motojima, M Fujiwara,
A Study of High-Energy Ions Produced by ICRF Heating in LHD Sep 2001

NIFS-713 Y. Matsumoto, S.-I Oikawa and T. Watanabe,
Field Line and Particle Orbit Analysis in the Periphery of the Large Helical Device, Sep 2001

NIFS-714 S Toda, M. Kawasaki, N Kasuya, K. Itoh, Y Takase, A Furuya, M Yagi and S -I Itoh,
Contributions to the 8th IAEA Technical Committee Meeting on H-Mode Physics and Transport Barriers (5-7 September 2001, Toki, Japan) Oct 2001

NIFS-715 A Maluckov, N Nakajima, M Okamoto, S Murakami and R. Kanno,
Statistical Properties of the Particle Radial Diffusion in a Radially Bounded Irregular Magnetic Field, Oct 2001

NIFS-716 Boris V Kuteev,
Kinetic Depletion Model for Pellet Ablation, Nov 2001

NIFS-717 Boris V Kuteev, Lev D. Tsendin,
Analytical Model of Neutral Gas Shielding for Hydrogen Pellet Ablation Nov 2001

NIFS-718 Boris V Kuteev,
Interaction of Cover and Target with Xenon Gas in the IFE-Reaction Chamber Nov 2001